Time-Resolved SAXS, WAXS, and DSC Study of Melting of Poly(aryl ether ether ketone) (PEEK) Annealed from the Amorphous State

C. Fougnies,[†] P. Damman,[§] M. Dosière,*[,†] and M. H. J. Koch[‡]

Laboratoire de Physicochimie des Polymères, Université de Mons-Hainaut, Place du Parc 20, B-7000 Mons, Belgium, and European Molecular Biology Laboratory, Hamburg Outstation, EMBL c/o DESY, Notkestrasse 85, D-22603 Hamburg, Federal Republic of Germany

Received August 1, 1996; Revised Manuscript Received December 12, 1996[⊗]

ABSTRACT: The melting behavior of semicrystalline samples of PEEK crystallized from the glassy state was investigated by differential scanning calorimetry (DSC) and simultaneous time-resolved small-angle (SAXS) and wide-angle (WAXS) X-ray diffraction. The long spacing L and the invariant were computed from the Lorentz SAXS intensity curves. The amorphous L_a and crystalline L_c thickness as well as the linear degree of crystallinity v_c^{lin} were obtained from the correlation function $\gamma(r)$. The wide-angle and small-angle integrated intensities were correlated to the degree of crystallinity obtained by DSC throughout the melting. The double-melting behavior of samples prepared by annealing at temperatures below 315 °C can be attributed to a melting−recrystallization process of a single population of crystals. The structural parameters of the reorganized lamellae in the different samples become identical as soon as the temperature exceeds the annealing temperature. Annealing at temperatures corresponding to the second melting point region (340 °C) generates a sample containing two populations of lamellae with a melting behavior very different from that of the samples prepared at lower temperatures.

Introduction

It is generally accepted that the macroscopic properties of semicrystalline polymers are governed by their microscopic morphology, which in turn depends on their crystallization conditions and on their thermal history. For this reason, the melting behavior of high-performance polymers including poly(ethylene terephthalate) (PET), poly(phenylene sulfide) (PPS), poly(butylene terephthalate) (PBT), and poly(ether ether ketone) (PEEK) have been widely studied during the last decade.[1−11] For PET, PPS, and PBT, a second melting endotherm was observed at low temperature when cold-crystallized polymer films were annealed. On the basis of DSC investigations, several authors have attributed this second endotherm to a recrystallization process occurring during the annealing and/or the melting of the sample. The superposition of a recrystallization exotherm and of a broad melting endotherm was also considered to explain the pair of endothermic peaks.[9−11] The occurrence of two endotherms in the melting curves of semicrystalline PEEK samples was first described by Blundell et al.[1] and has been correlated with a two-stage drop of the Young's modulus.[2] Two hypotheses, essentially based on differential scanning calorimetry analyses, were put forward: (i) the semicrystalline PEEK sample is made of only one population of crystals which reorganize during heating to finally melt around 340 °C[1]; (ii) the two endotherms are associated with two distinct lamellar populations which coexist in the sample prior to the DSC heating scan.[6] The double-melting behavior is still not fully understood and there is no general consensus on its origin. In particular, the question whether the high melting point crystals (340 °C) exist before the heating scan or result from a recrystallization process is still open.

In addition to the usual DSC experiments, time-resolved SAXS and WAXS were also used to characterize the semicrystalline morphology of PEEK during crystallization and melting.[2,12−15] An investigation of the melting of samples crystallized in steps from the melt and exhibiting multiple endotherms revealed that each step in crystallization temperature T_c was associated with an increase of the long period during heating.[14] This result was attributed to the melting of different populations of increasingly perfect crystals grown at different T_c steps. Correlation function analysis was extensively used to probe the evolution of the lamellar morphological parameters in order to understand the crystallization and melting mechanisms of PEEK.[12,13,15] The occurrence of multiple peaks in the SAXS intensity profiles led to a dual lamellar model in which dominant lamellae grow during the first stage of the crystallization whereas during the second step infilling lamellae crystallize between those formed during the first step. The relative amount, exact location, and dimensions of these secondary lamellae remain, however, to be defined. The reversibility of the structural parameters of PEEK samples submitted to heating and cooling cycles up to 300 °C was also investigated.[2] The results could be fully explained by assuming the existence of a single population of lamellae. Unfortunately, the second melting region above 300 °C, where important morphological modifications occur,[16,17] was not studied due to experimental limitations. Most of the conclusions of the above investigations were drawn from the analysis of the correlation function. This technique has been successfully applied to highly crystalline polymers like polyethylene.[18,19] It is questionable that the implicit "two-phase model" with sharp boundaries would correctly describe the semicrystalline morphology of PEEK. The controversy concerning the assignment of the linear degree of crystallinity v_c^{lin} further emphasizes the need for systematic studies to understand the

* To whom correspondence should be addressed.
[†] Université de Mons-Hainaut.
[‡] European Molecular Biology Laboratory.
[§] Research Associate of the Belgian National Fund for Scientific Research.
[⊗] Abstract published in *Advance ACS Abstracts,* February 1, 1997.

S0024-9297(96)01151-5 CCC: $14.00

mechanism of crystallization and melting in PEEK.[2,15]

In a previous paper,[20] we have shown that the annealing of amorphous PEEK above around 315 °C yields samples in which two distributions of crystals coexist. The first one grows during the isotherm while the second one crystallizes during subsequent cooling. When the samples are prepared at lower temperatures, there is no significant crystallization during cooling and the resulting samples contain only lamellae crystallized during the heating to the annealing and during isothermal conditions. The present paper is devoted to a comparative melting study of PEEK samples prepared at temperatures between 280 and 340 °C chosen to obtain relative magnitudes of the low-temperature endotherm (called hereafter endotherm I) that differ as much as possible from one sample to the next and amount to up to 50% of the total melting enthalpy.

Experimental Section

PEEK Stabar K200 was obtained from ICI (U.K.) in the form of 260 μm thick films. The reported $\bar{M}_n$ and $\bar{M}_w$ average molecular weights range from 35 000 to 50 000 and 95 000 to 120 000, respectively. The films were amorphous as indicated by the absence of any crystalline reflections or preferred orientation in their wide-angle X-ray scattering patterns. Semicrystalline samples were prepared by heating pieces of these films wrapped between aluminum foils from room temperature to the annealing temperature T_a at 10 °C/min in a Mettler FP82 hot stage. After an annealing time of 1 h, each sample was cooled to room temperature at −10 °C/min. The density of the annealed samples was measured by the flotation technique at 25 °C using aqueous $Ca(NO_3)_2$ solutions. The density of the solutions was measured with a Mettler DA 110 densimeter with an accuracy of 10^{-3} g·cm^{-3}. The starting material has a density of 1.263 g·cm^{-3}, which is in good agreement with previously reported values for amorphous PEEK.[1,5,7] The weight degree of crystallinity was estimated in the standard way, taking into account the dependence of the crystal density on the crystallization temperature.[21−23]

The DSC measurements were made in a Perkin-Elmer DSC4 calorimeter under nitrogen. Temperature and heat flow calibrations were done using caffeine, indium, zinc, and lead. The melting temperatures (T_m) and melting enthalpies (ΔH) are given to an accuracy of 0.5 °C and 1 J/g, respectively. The errors are defined by the standard deviation observed for T_m and ΔH measured for PEEK films annealed at 280 °C. A new baseline was recorded by running two empty pans before each experiment. The melting enthalpy of PEEK was taken as the area over a linear baseline drawn from just above the glass transition (165 °C) to 360 °C.[24] The weight degree of crystallinity was computed using a value of 130 J·g^{-1} for the crystalline melting enthalpy of PEEK.[1]

Time-resolved diffraction experiments were done on the X33 beamline of the EMBL in HASYLAB on the storage ring DORIS III of the Deutsches Elektronen Synchrotron DESY at Hamburg (Federal Republic of Germany).[25,26] The wavelength λ of the incident X-ray beam is 0.154 nm. A Mettler FP82HT hot stage was used to heat the samples wrapped in 50 μm aluminum foils in the X-ray beam. The SAXS and WAXS intensity curves were simultaneously recorded with two linear position sensitive detectors mounted in series.[27] The s range ($s = 2 \sin \theta/\lambda$) of the WAXS detector was calibrated with benzoic acid, biphenyl, and naphthalene and covers the range between 1.7 and 3.6 nm^{-1}. The distance between the sample and the SAXS linear position detector was 400 cm. The SAXS Bragg window was calibrated with rat tail collagen and ranges from $s = 1/70$ to $1/3$ nm^{-1}. The WAXS and SAXS intensity curves were normalized to the primary X-ray beam intensity using the signal of an ionization chamber placed in front of the sample. The SAXS and WAXS profiles were Lorentz corrected by multiplication by s^2 and $\sin 2\theta \sin \theta$, respectively. Errors on the long periods are defined by the distance between two channels (e.g. at 15 nm, the error is equal to 0.1 nm). The correlation functions $\gamma(r)$ were calculated from the corrected SAXS intensity curves after subtraction of the fluidlike contribution and extrapolation to high s values using the Porod law.[28] The morphological parameters such as the crystalline (L_c) and amorphous (L_a) thicknesses and the linear degree of crystallinity (v_c^{lin}) were derived from the correlation function using the standard procedure.[18,19]

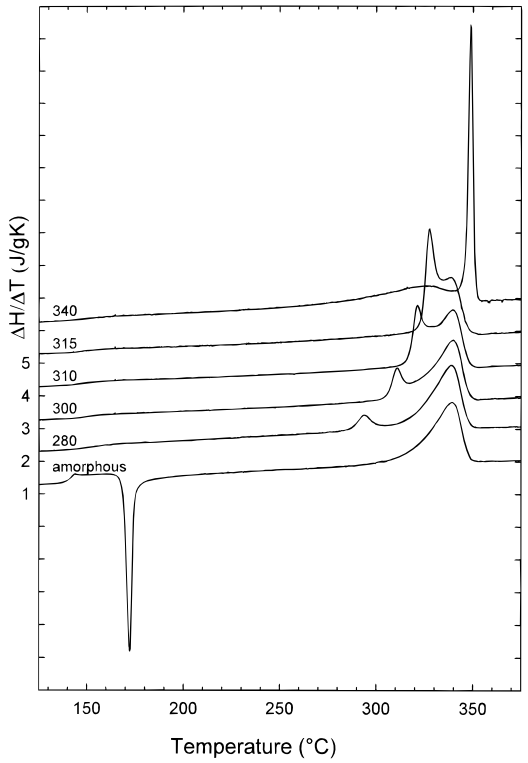

Figure 1. DSC traces of amorphous and semicrystalline PEEK samples prepared at different temperatures. Successive traces have been shifted by 1 J/g·K along the ordinate for better visualization. The vertical axis refers to the bottom curve.

Results and Discussion

Differential Scanning Calorimetry. The DSC melting traces of the amorphous starting material and of the different semicrystalline PEEK samples, recorded with a heating rate of 10 °C·min^{-1}, are shown in Figure 1. The first four semicrystalline samples crystallized at 280, 300, 315, and 340 °C exhibit a characteristic double-melting behavior with a first melting endotherm (endotherm I) appearing around 15 °C above the annealing temperature T_a and a second one (endotherm II) peaking at 340 °C independently of the annealing temperature. Comparison of the melting traces of these annealed samples with that of amorphous PEEK reveals that (i) the glass temperature T_g is shifted to higher temperature; (ii) the crystallization exotherm has, as expected, disappeared; (iii) endotherm I appears and progressively shifts to higher temperatures with increasing annealing temperature; and (iv) endotherm II is present in all DSC traces. Its maximum appears between 338 and 340 °C. Its shape is identical for the initially amorphous film and for the samples annealed at 280, 300, 310, and 315 °C even if partly masked by endotherm I. Other results show that for samples prepared from the glass between 150 and 315 °C, the shape of the second endotherm is independent of their thermal history if crystallization time is sufficiently short to avoid degradation of the polymer.

The melting curve of the PEEK sample annealed at 340 °C also displays two endotherms. The low-temper-

Table 1. Thermal Properties, Density, Long Period, Lamellar Thickness, and Degree of Crystallinity of Annealed Samples of PEEK[a]

	DSC							density		SAXS			
sample	heating rate (°C/min)	T_m^1 (°C)	T_m^2 (°C)	ΔH_f^1 (J/g)	ΔH_f^2 (J/g)	ΔH_f^{tot} (J/g)	W_c (DSC) (%)	density (g/cm^3)	W_c (density) (%)	L^{Bragg} (nm)	L^{corr} (nm)	ν_c^{lin}	L_c (nm)
amorph	2		343.0					1.263	0				
	5		342.0										
	10		340.0										
	20		339.0										
	40		339.5										
	80		337.0										
280/60	2	289.5	343.0	3.5	39.3	42.8	32.9	1.301	31.2	11.5	11.3	0.28	3.1
	5	292.5	341.0	5.2	36.1	41.3	31.8						
	10	293.5	339.0	7.2	35.3	42.5	32.7						
	20	296.0	338.0	8.9	34.3	43.2	33.2						
	40	299.5	336.5	8.1	32.9	41.0	31.5						
	80	303.5	337.5	8.2	32.8	41.0	31.5						
300/60	2	308.0	343.0	2.2	39.2	41.4	31.8	1.303	32.5	12.0	11.5	0.28	3.2
	5	310.0	341.0	3.6	41.3	44.9	34.5						
	10	312.0	340.0	4.2	39.9	44.1	33.9						
	20	314.5	339.0	5.3	37.0	42.3	32.5						
	40	316.5	337.0	15.3	27.4	42.7	32.8						
	80	324.0	338.0	22.1	19.1	41.2	31.7						
310/60	2	319.0	342.5	4.6	40.7	45.3	34.8	1.305	34.1	12.7	12.5	0.29	3.6
	5	321.0	341.0	15.8	30.7	46.5	35.8						
	10	322.0	339.0	22.6	23.0	45.6	35.1						
	20	324.0	338.0	28.0	17.2	45.2	34.8						
	40	327.5	337.5	33.1	12.4	45.5	35.0						
	80[b]		334.0		46.0	46.0	35.4						
315/60	2	326.0	342.5	12.8	36.4	49.2	37.9	1.306	34.9	12.9	12.5	0.29	3.6
	5	327.0	340.5	27.3	20.0	47.3	36.4						
	326.0	338.0	30.0	17.7	47.7	36.7							
	20	329.0	337.0	34.5	12.3	46.8	36.7						
	40	330.0	337.0	34.9	13.9	48.8	37.5						
	80[b]		336.0		46.5	46.5	35.8						
340/60	2	330.0	347.0	28.5	23.3	51.8	39.8	1.313	40.3	15.3	15.4	0.31	4.8
	5	330.0	350.0	30.7	23.3	54.0	41.5						
	10	328.0	351.0	33.1	19.6	52.7	40.5						
	20	326.0	352.5	33.7	20.6	54.3	41.2						
	40	327.0	354.5	30.1	21.2	51.3	39.4						
	80	326.0	358.5	31.2	21.1	52.3	40.2						

[a] The long periods were measured at 100 °C and computed either from the Bragg peak position or from the correlation function analysis. [b] Only one endotherm in the DSC curve.

ature endotherm is very broad with a maximum at 328 °C, a value well below the annealing temperature. The sharp extremum of the high-temperature endotherm (endotherm II) at 352 °C indicates the presence of perfect lamellar crystals of uniform thickness.

Melting curves at different scanning rates ranging between 2 and 80 °C·min^{-1} were also recorded to investigate possible reorganization effects during the heating in the DSC scans. The characteristic temperatures of endotherms I and II (T_I and T_{II}), the partial melting heats of endotherms I and II (ΔH_I and ΔH_{II}), and the total melting heat are given in Table 1. The samples prepared between 280 and 315 °C display the same behavior with respect to the heating rate as illustrated in Figure 2a for PEEK annealed at 280 °C. Both the temperature (T_I) and the partial melting heat (ΔH_I) of endotherm I increase with the heating rate whereas the opposite trends are observed for the corresponding parameters of endotherm II. These results are consistent with previous observations[5] and in sharp contrast with those obtained for the film annealed at 340 °C, where the reverse situation is observed (Figure 2b). For this last sample, endotherm I moves to lower temperature and endotherm II shifts upward with higher heating rates while their relative melting heats remain almost constant (Table 1). The opposite evolution of T_I and T_{II} for amorphous PEEK samples annealed at 280 and 340 °C is clearly illustrated in Figure 3. The melting behavior of the first four semicrystalline samples can be explained by a reorganization process. The first endotherm is the result of two opposite contributions: melting and recrystallization processes. If the heating rate is increased, the time left for the recrystallization step is shorter and its exothermic contribution will therefore be reduced. The net result is an increase of the temperature T_I and the partial melting heat ΔH_I. Simultaneously, as the reorganized lamellae are less perfect, the extremum of the high-temperature endotherm (T_{II}), which is associated with their melting, shifts to lower temperatures and as the amount of recrystallized material decreases, so does the partial area ΔH_{II} of endotherm II. It can be excluded that this behavior would be caused by an artifact due to thermal conductivity of the polymer since this should lead to an increase of the temperature of both endotherms with the heating rate.

The sample annealed at 340 °C contains two types of lamellar crystals in approximately equal amounts. The thicker lamellae have grown during the isotherm while the thinner ones were formed during the cooling phase. These imperfect crystals have grown in a restricted environment between the previous existing crystals made at 340 °C, which strongly impede their reorganization upon heating. The lower endotherm represents the melting of these poorly crystalline lamellae which reorganize only to a small extent. As the rearrangement of the thicker crystals in the second melting temperature range (350 °C) seems very unlikely, the upward

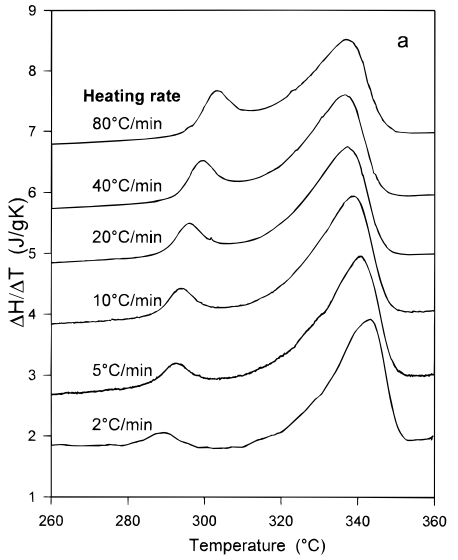

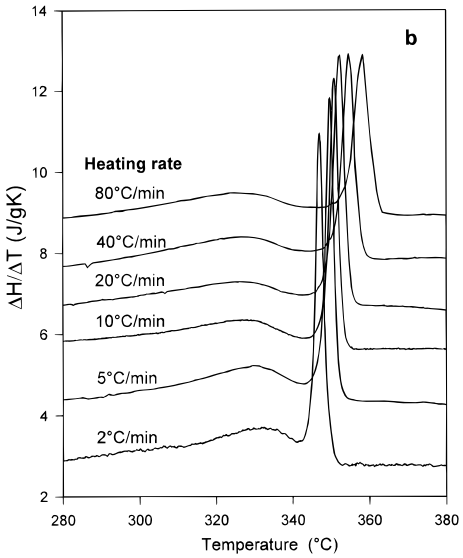

Figure 2. DSC melting traces recorded with different heating rates (as indicated) of the samples prepared at 280 (a) and 340 °C (b). The vertical axis refers to the bottom curve; the other traces were displaced along the ordinate for better visualization.

temperature shift of this endotherm with increasing scan rate is attributed to the lag resulting from the poor thermal conductivity of the polymer.

X-ray Diffraction. Figure 4 shows the background-subtracted time-resolved SAXS and WAXS data recorded during heating of the PEEK sample prepared at 280 °C.

Wide-Angle X-ray Diffraction. The evolution of the orthorhombic lattice parameters and of the crystal density ρ_c computed from the spacings of the WAXS reflections is given in Figure 5 as a function of temperature. The lattice expands predominantly along the *a*-crystallographic parameter, which is consistent with the weaker attractive interactions between chains along the (100) direction. Although the temperature dependence of the crystal density ρ_c is nonlinear, the average value of the crystal expansion coefficient between 150 and 300 °C is found to be 2.3×10^{-4} K^{-1}, in good agreement with values reported earlier.[2,29,30] The value of the expansion coefficient does not depend on the preparation temperature, and no polymorphism was observed even for the sample prepared at 340 °C. A

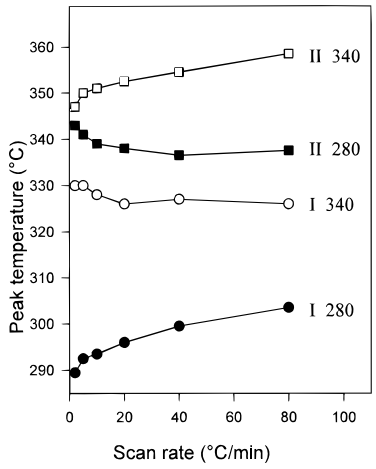

Figure 3. Evolution of the first peak (○, ●) and second peak (□, ■) maximum with the DSC scan rate for the sample prepared at 280 (filled symbols) and 340 °C (open symbols).

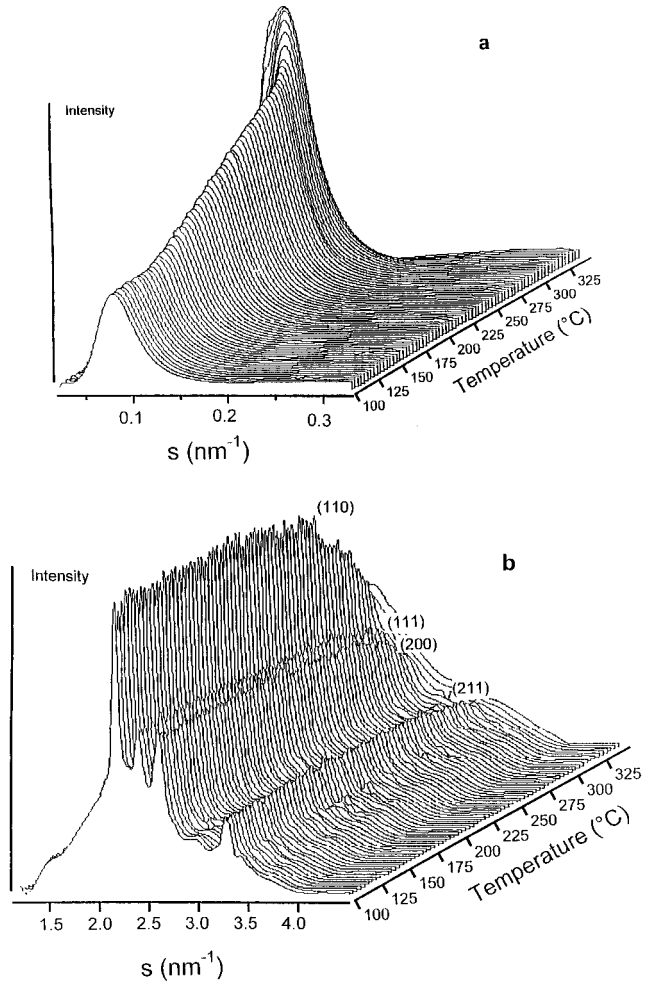

Figure 4. Background-subtracted SAXS (a) and WAXS (b) intensities recorded during the melting of the sample prepared at 280 °C.

crystallinity index A_c can be estimated from the WAXS patterns by dividing the peak areas of the (110), (200), (111), and (211) reflections by the total scattered intensity after deconvolution. For samples at room temperature, A_c correlates well with the weight degree of crystallinity obtained from density measurements. However, as there are discrepancies between those quantities at other temperatures, A_c will only be used here as a relative quantity.

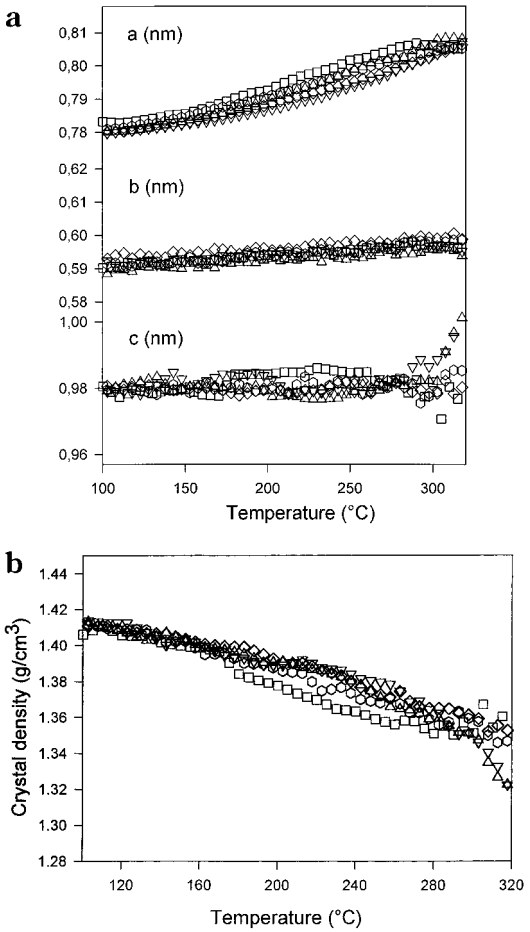

Figure 5. Evolution of the lattice parameters *a*, *b*, and *c* (a) and of the crystal density ρ_c (b) during heating at 10 °C/min of semicrystalline samples prepared at 280 (□), 300 (△), 310 (▽), 315 (◇), and 340 °C (⬡).

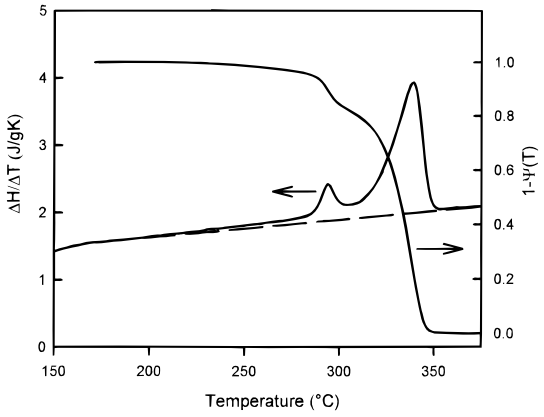

Figure 6. Estimation of the relative amount of unmolten material $1 - \Psi(T)$ as a function of T from the DSC signal for a sample prepared at 280 °C. The dashed line represents the baseline above which the integration has been performed.

In a recent DSC, SAXS, and WAXS study of the melting of PEEK samples obtained by stepwise crystallization from the melt, the DSC curve was correlated with the derivative of crystalline diffracted intensity dA_c/dT.[14] As this derivative is very sensitive to noise and thus requires preliminary smoothing of the experimental curves, we prefer to compare the DSC curve with A_c using the following procedure (see Figure 6). Integration of the DSC signal above the baseline and division by the total melting enthalpy yields the relative amount $\Psi(T)$ of crystals molten at the temperature T;

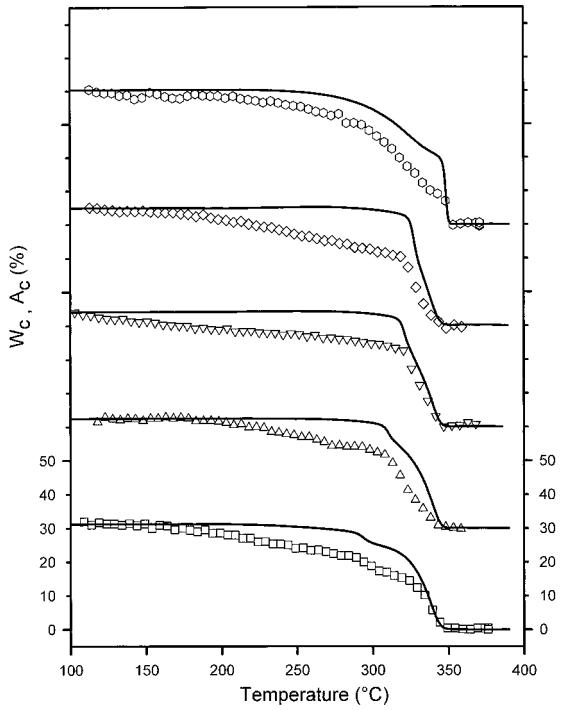

Figure 7. Evolution of the weight degree of crystallinity estimated from the DSC curve ($W_c = W_c^0(1 - \Psi(T))$) (solid lines) and of I_{WAXS} (open symbols) during the melting at 10 °C/min of the different samples. To allow comparison, the values of A_c have been scaled so that both curves match at 100 °C. The vertical axis refers to the bottom curve ($T_a = 280$ °C); the other curves are shifted for clarity (280 (□), 300 (△), 310 (▽), 315 (◇), and 340 °C (⬡)).

thus $\Psi(100\ °C) = 0$ and $\Psi(360\ °C) = 1$. If the initial weight degree of crystallinity W_c^0 is known from DSC or from density measurements (these values are in good agreement as illustrated in Table 1), $W_c(T) = W_c^0(1 - \Psi(T))$ represents the degree of crystallinity of the sample as a function of temperature. The evolution of A_c and W_c are plotted together in Figure 7 as a function of the temperature. For all the samples investigated here, A_c is found to decrease more rapidly than expected from the DSC curve even in the low-temperature region where no melting occurs. This unexpected decrease is mainly due to thermal motion and can account for tens of percents at high temperature (see Figure 7). This phenomenon can obviously not be neglected in the analysis of the WAXS intensity as a function of T. It is thus necessary to determine the degree of crystallinity independently by calorimetry, for instance. Note that this problem is not encountered in the SAXS analysis given below.

The two endotherms in the double-melting region of the DSC curve are associated with the two-stage decrease of A_c. For the sample annealed at 340 °C, melting occurs over a wider range of temperature and $W_c(T)$ starts to decrease significantly above 250 °C. At 340 °C only 50% of the crystals are molten and the remaining lamellae corresponding to the narrow peak in the DSC trace melt between 340 and 352 °C.

Small-Angle X-ray Scattering. The temperature dependence of the long period L of the different samples determined from the position of the maximum of the Lorentz-corrected SAXS curves is shown in Figure 8. During heating, the long period of the first four semicrystalline samples increases moderately up to the annealing temperature T_a. Around $T_a + 15$ °C, the curves become steeper and all coincide with the one

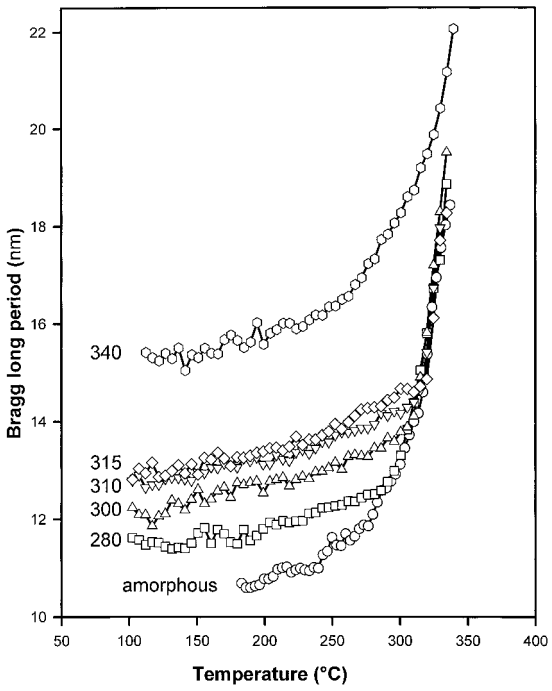

Figure 8. Evolution of the Bragg long spacing L during heating at 10 °C/min of the amorphous sample and of the five semicrystalline samples.

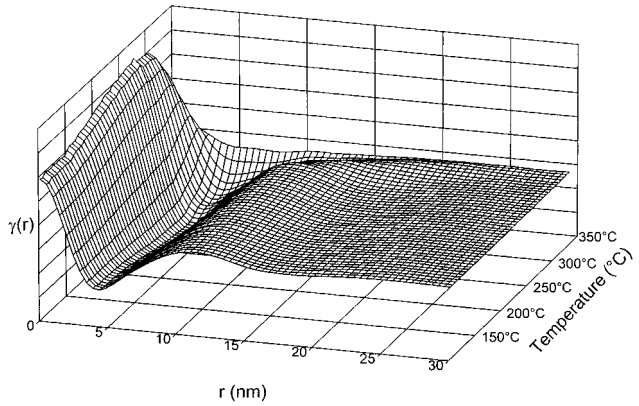

Figure 9. Correlation functions $\gamma(r)$ obtained from the SAXS intensities recorded during heating at 10 °C/min of a semicrystalline sample prepared at 280 °C.

obtained during heating of an amorphous sample. In contrast, the long spacing of the sample annealed at 340 °C continuously increases over the whole range of temperature from 250 to 340 °C and never overlaps with the other curves. The crystalline and amorphous thicknesses L_c and L_a and the linear degree of crystallinity $v_c^{lin} = L_c/(L_c + L_a)$ were computed from the correlation function. An example of the evolution of this function during the melting of the sample previously annealed at 280 °C is illustrated in Figure 9. For a two-phase model with sharp boundaries, the analysis of the correlation function $\gamma(r)$ yields the thicknesses of the two successive zones, which, as a result of Babinet's principle, however cannot be assigned unambiguously to the amorphous or crystalline regions on the basis of SAXS experiments alone.[2] There is still some controversy about this assignment, some authors having chosen the largest length to characterize the thickness of the crystalline zones[12,13,15] while others used the reverse picture.[2] Numerous arguments were given in support of either of these hypotheses. As justified earlier for PEEK annealed from the glassy state,[20] we have assigned the smallest length to the crystalline zones. Figure 10 illustrates the evolution of L_a, L_c, and v_c^{lin} during the heating of an amorphous film and semicrystalline samples prepared at 280, 310, and 340 °C. At 100 °C, L_c and L_a increase with the annealing temperature (Table 1). L_a increases relatively less than L_c, and v_c^{lin}, as expected, also increases with the annealing temperature. The structural parameters of the first four semicrystalline samples behave similarly during heating. In the 100 °C to the annealing temperature range, L_a and L_c increase because of thermal expansion, leading to an almost constant value of v_c^{lin}. Above T_a + 15 °C, the slopes of the curves change abruptly. L_a now increases relatively more than L_c, and v_c^{lin} diminishes. This may be interpreted as follows: above the annealing temperature, most of the original crystals have completely melted while others reorganize into thicker lamellae. Consequently, the amorphous gap separating the reorganized crystals is larger. Note that the final parts of the curve giving the evolutions of L_c, L_a, and v_c^{lin} vs T are identical for the first four samples and superimposed with the data collected during the heating of an initially amorphous film. This is consistent with the WAXS results and with the shape similarity of the second endotherm already mentioned above for the amorphous and the first four semicrystalline samples. These results strongly suggest that a reorganization process takes place during which the reorganized lamellae become identical as soon as the crystals present in the sample at room temperature have melted, i.e. shortly after the first endotherm. On this account, the second endotherm results from the melting of a similar distribution of reorganized crystals. If one accepted the second hypothesis regarding the origin of the double-melting behavior, one would have difficulties in explaining how lamellae crystallized in different ways and having probably different morphologies would have an identical melting behavior.

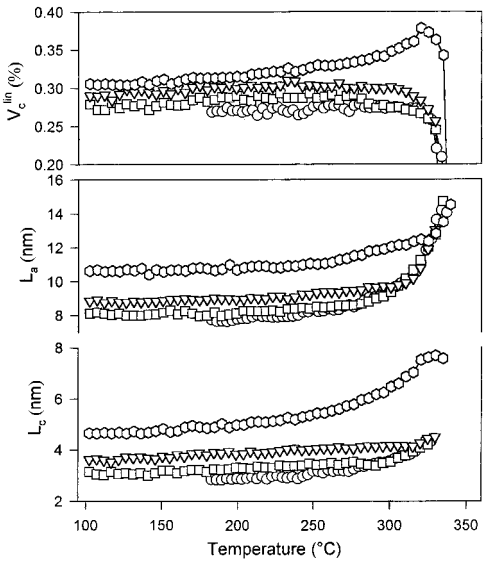

Figure 10. Evolution of the linear crystallinity v_c^{lin} and of the crystalline (L_c) and amorphous (L_a) thicknesses during heat at 10 °C/min of an amorphous sample (○) and of the semicrystalline samples prepared at 280 (□), 310 (▽), and at 340 °C (○).

The trends of L_a and L_c for the last sample (T_a = 340 °C) are very different (Figure 10); both values increase with temperature in the 100−320 °C temperature range, leading to a higher value of the linear crystallinity v_c^{lin}. In this case, the measured values are averaged over two

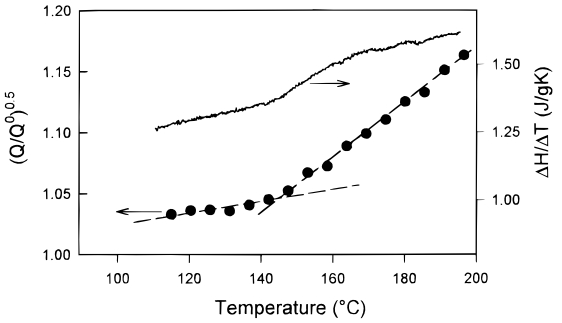

Figure 11. Plot of $(Q/Q^0)^{0.5}$ and DSC curve versus temperature during heating at 10 °C/min of the sample prepared at 280 °C. Note the break at the glass transition.

lamellar populations that have grown, one in isothermal and the other in nonisothermal conditions. The imperfect crystals characterized by a relatively small L_c and v_c^{lin} are progressively removed (broad endotherm) with the consequence that L_c slowly increases over this temperature range. The crystals remaining at high temperature are the perfect ones characterized by high crystal length and linear crystallinity. The melting of this last population leads to the decrease of v_c^{lin} observed during the final part of the heating phase.

The invariant Q was calculated directly from the intensity curves after background subtraction. This is justified insofar as the contribution of the experimental data is the dominant term in the traditional way of calculating the invariant[31] and we are here only concerned with relative values. The fact that the amorphous thermal expansion coefficient α_a jumps in the region of the glass transition around 145 °C while the crystalline expansion coefficient α_c remains constant allows one to estimate the glass transition temperature T_g and α_a for a semicrystalline system.[32] The invariant at a reference temperature $T^0 < T_g$ can be expressed as

$$Q^0 = K v_l^0 v_c^{0,lin}(1 - v_c^{0,lin})(\rho_a^0 - \rho_c^0)^2 \qquad (1)$$

where v_l^0, $v_c^{0,lin}$, ρ_c^0, and ρ_a^0 are the fraction of the material transformed into stacks, the linear degree of crystallinity, and the crystalline and amorphous electron densities at T^0, respectively. K is a conversion constant between electron and macroscopic densities. At a temperature T this expression becomes

$$Q = K v_l v_c^{lin}(1 - v_c^{lin})(\rho_a - \rho_c)^2 \qquad (2)$$

If neither v_l nor v_c^{lin} change between T^0 and T, a plot of $(Q/Q^0)^{0.5}$ will consist of two linear regions with different slopes intersecting at T_g as illustrated in Figure 11 for one of the samples. Two successive heating and cooling cycles with a maximum temperature of $T_a - 20$ °C were applied to similar samples, and the changes of L and Q were found to be entirely reversible, thereby proving that no morphological modifications other than those induced by thermal expansion occur. This method allows us to determine $[\Delta\rho(T)]^2$ used in the following relationship to compute the corrected scattering power Q_{cor}, which no longer depends on differential thermal expansion effects: $Q_{cor} = Q/[\Delta\rho(T)]^2$. The thermal evolution of Q_{cor} is shown in Figure 12 (open symbols) for the different samples investigated here. From Figures 10 and 12, v_c^{lin} and Q_{cor} remain constant as long as the temperature remains lower than T_a, implying that v_l does not change. Above T_a, Q_{cor} decreases in two steps corresponding to the double

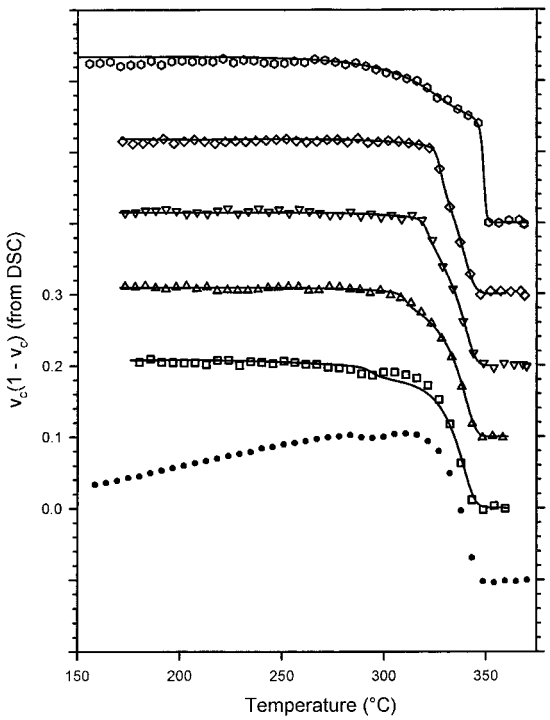

Figure 12. Evolution of the corrected invariant Q_{cor} (open symbols) with temperature during the heating at 10 °C/min of the various samples prepared at 280 (□), 300 (△), 310 (▽), 315 (◇), and 340 °C (⬡). The solid lines represent the evolution of $v_c(1 - v_c)$ obtained from the DSC data. The vertical axis refers to the curve corresponding to the melting of the sample annealed at 280 °C; the other curves are shifted along the ordinate for clarity. The Q values are scaled to $v_c(1 - v_c)$ at 100 °C in order to facilitate the comparison. The filled symbols represent the evolution of the invariant uncorrected for the differential expansion behavior of the crystalline and amorphous zones for a sample prepared at 280 °C. This curve is shifted downward.

melting recorded by DSC. The thermal evolution of the macroscopic volume degree of crystallinity v_c can also be estimated from the DSC thermograms using the following relationship

$$v_c(T) = \left[1 + \frac{1 - w_c(T)}{w_c(T)} \frac{\rho_c(T)}{\rho_a(T)}\right]^{-1} \qquad (3)$$

where $W_c(T)$ is computed as described above. The product $v_c(1 - v_c)$ can thus be estimated from the DSC experiment and is plotted as a function of the temperature in Figure 12 (solid lines). The near-perfect matching of both sets of curves clearly indicates the absence of isolated lamellae whose melting could be observed by DSC but would not contribute to the scattering power. Q_{cor} thus accounts for all the crystalline material. Moreover, the evolution of v_c^{lin} is in very good agreement with that of the macroscopic volume fraction crystallinity v_c. This indictes that heating the amorphous polymer through the cold crystallization generates a sample where the crystalline order is very poor with stacks containing only a few lamellae and with a relatively small lateral extension.

Conclusions

The double-melting behavior of semicrystalline PEEK prepared by annealing from the glassy state below 315 °C is due to a reorganization process of the lamellae formed at the preparation temperature. The thermal history of the sample is erased as soon as the temper-

ature exceeds the annealing temperature T_a by a few degrees. Above T_a, the morphological parameters of the reorganizing lamellae are identical for all samples and coincide with those obtained during the heating of an amorphous film in the same temperature range. As a result, the shape of the second endotherm is also similar for all these samples. In contrast, the film prepared at 340 °C contains two lamellar populations which give rise to two independent endotherms in the DSC heating curve. The evolution of the structural parameters which are averaged over the two crystal distributions is very different from the previous cases. Finally, the corrected invariant Q_{cor} during heating correlates very well with $v_c(1 - v_c)$ calculated from the DSC curve whereas the WAXS crystallinity index A_c deviates at high temperature from the value (W_c) found by DSC due to thermal motion.

Acknowledgment. This work was supported by the Belgian National Fund for Scientific Research and the European Union through the HCMP Access to Large Installations Project, Contract No. CHGE-CT93-0040.

References and Notes

(1) Blundell, D. J.; Osborn, B. N. *Polymer* **1983**, *24*, 953.
(2) Jonas, A. M.; Russell, T. P.; Yoon, D. Y. *Macromolecules* **1996**, *28*, 8491.
(3) Cheng, S. Z. D.; Cao, M.-Y.; Wunderlich, B. *Macromolecules* **1986**, *19*, 1868.
(4) Blundell, D. J. *Polymer* **1987**, *28*, 2248.
(5) Lee, Y.; Porter, R. S. *Macromolecules* **1987**, *20*, 1336.
(6) Bassett, D. C.; Olley, R. J.; Al Raheil, I. A. M. *Polymer* **1988**, *29*, 1745.
(7) Cebe, P. *J. Mater. Sci.* **1988**, *23*, 3721.
(8) Lee, Y.; Porter, R. S.; Lin, J. S. *Macromolecules* **1989**, *22*, 1756.
(9) Yeh, J. T.; Runt, J. *J. Polym. Sci., Part B: Polym. Phys.* **1989**, *27*, 1543.
(10) Chung, J. S.; Cebe, P. *J. Polym. Sci., Part B: Polym. Phys.* **1992**, *30*, 163.
(11) Kim, J.; Nichols, M. E.; Robertson, R. E. *J. Polym. Sci., Part B: Polym. Phys.* **1994**, *32*, 887.
(12) Hsiao, B. S.; Gardner, K. H.; Wu, D. Q.; Chu, B. *Polymer* **1993**, *34*, 3986.
(13) Hsiao, B. S.; Gardner, K. H.; Wu, D. Q. *Polymer* **1993**, *34*, 3996.
(14) Krüger, K.-N.; Zachmann, H. G. *Macromolecules* **1993**, *26*, 5202.
(15) Hsiao, B. S.; Sauer, B. B.; Verma, R. K.; Zachmann, H. G.; Seifert, S.; Chu, B.; Harney, P. *Macromolecules* **1996**, *28*, 6931.
(16) Lovinger, A. J.; Davis, D. D. *Macromolecules* **1986**, *19*, 1861.
(17) Marand, H.; Prasad, A. *Macromolecules* **1992**, *25*, 1731.
(18) Strobl, G. R.; Schneider, M. J. *J. Polym. Sci., Polym. Phys. Ed.* **1980**, *18*, 1343.
(19) Strobl, G. R.; Schneider, M. J.; Voigt-Martin, I. G. *J. Polym. Sci., Polym. Phys. Ed.* **1980**, *8*, 1361.
(20) Fougnies, C.; Damman, P.; Villers, D.; Dosière, M.; Koch, M. H. J. *Macromolecules* **1997**, *30*, 1385.
(21) Zimmermann, H. J.; Könnecke, K. *Polymer* **1991**, *32*, 1962.
(22) Wakelyn, N. T. *J. Polym. Sci., Polym. Lett.* **1987**, *25*, 25.
(23) Hay, J. N.; Langford, J. I.; Lloyd, J. R. *Polymer* **1989**, *30*, 489.
(24) Sichina, W. J. *24th NATAS Conf. Proc.* **1995**, 375.
(25) Boulin, C. F.; Kempf, R.; Koch, M. H. J.; McLaughin, S. M. *Nucl. Instrum. Methods* **1986**, *A249*, 399.
(26) Boulin, C. F.; Kempf, R.; Gabriel, A.; Koch, M. H. J. *Nucl. Instrum. Methods* **1988**, *A269*, 312.
(27) Rapp, G.; Gabriel, A.; Dosière, M.; Koch, M. H. J. *Nucl. Instrum. Methods* **1995**, *A357*, 178.
(28) Balta-Calleja, F. J.; Vonk, C. G. In *X-ray Scattering of Synthetic Polymers*; Elsevier: Amsterdam, 1989; Chapter 7.
(29) Blundell, D. J.; D'Mello, J. *Polymer* **1991**, *32*, 304.
(30) Zoller, P.; Hehl, T.; Starkweather, H. W.; Jones, G. A. *J. Polym. Sci., Part B: Polym. Phys.* **1989**, *27*, 993.
(31) Russel, T. P. *Handbook on Synchrotron Radiation*; Brown, G. S., Moncton, D. E., Eds.; Elsevier: Amsterdam, 1991; Vol. 3, pp 379−469.
(32) Fischer, E. W.; Kloos, F. *J. Polym. Sci., Polym. Lett.* **1970**, *8*, 685.

MA961151I